

**Physically-motivated Recursively Embedded Atom Neural Networks:  
Incorporating Local Completeness and Nonlocality**

Yaolong Zhang, Junfan Xia, and Bin Jiang\*

*Hefei National Laboratory for Physical Science at the Microscale, Key Laboratory of  
Surface and Interface Chemistry and Energy Catalysis of Anhui Higher Education  
Institutes, Department of Chemical Physics, University of Science and Technology of  
China, Hefei, Anhui 230026, China*

\*: corresponding author: [bjiangch@ustc.edu.cn](mailto:bjiangch@ustc.edu.cn)

## Abstract

Recent advances in machine-learned interatomic potentials have largely benefited from the atomistic representation and locally invariant many-body descriptors. It was however recently argued that including three- (or even four-) body features is insufficient to distinguish some specific local environments. Utilizing an embedded density descriptor made by linear combinations of neighboring atomic orbitals and realizing that each orbital coefficient physically depends on its own local environment, we propose a recursively embedded atom neural network model. We formally prove that this model can efficiently incorporate complete many-body correlations without explicitly computing high-order terms. This model not only successfully addresses challenges of the local completeness and nonlocality in representative systems, but also provides a general way to adapt local descriptors to a message-passing form without changing their basic structures.

## Introduction

Over the past years, machine learning has achieved enormous success in many scientific fields, especially in the development of more accurate interatomic potentials based on ab initio data for chemical systems[1], including molecules and reactions[2-10], excited states[11-14], condensed phase materials[15-19], etc. Besides using different machine learning algorithms, these MLIPs mainly differ in their structural descriptors (or features) which should distinguish diverse molecular configurations and be invariant with respect to translation, rotation, and permutation of identical atoms. In small molecular and reactive systems, it is well-known that a global descriptor like permutationally invariant polynomials in terms of interatomic distances[8] of a sufficiently high order, or equivalently fundamental invariants[2], well satisfy both invariance and distinguishability requirements[20]. However, the size of polynomials scales factorially with the number of permutations, preventing their applications in large systems.

On the other hand, most MLIPs for large molecules and materials rely on an atomic decomposition of total energy, namely  $E = \sum_{i=1}^N E_i$ , as first proposed by Behler and Parrinello in their high-dimensional neural network (BPNN) approach[15]. In this representation, each atomic energy is dependent on the corresponding local environment (within a certain cutoff radius) described by a set of locally invariant representations of many-body interactions between the central and neighboring atoms[21-30]. Due to the high costs of evaluating higher-order terms, these local descriptors are typically truncated up to three- or four-body correlations. However, it

was recently shown that some local atomic structures in a system as small as  $\text{CH}_4$  become indistinguishable by the third (or even fourth) order correlations[31]. This would introduce a distortion of the feature space and intrinsically limit the representability of the MLIP[31]. While some approaches[27-29,32] could in principle resolve this structure degeneracy by systematically including higher-order terms, the computational cost would however increase dramatically.

An alternative way to describe an atom-centered environment is to repeatedly convolute feature vectors between every atom and its neighbors by neural networks (NNs) [6], allowing the information progressively passed among the central atom, the neighbors, the neighbors' neighbors, and so on so forth. Such so-called message-passing neural networks (MPNNs)[6,33,34] automatically learn an increasingly more sophisticated feature-property correlation from the training data. However, it is less clear that how this type of models incorporate many-body correlations by iteratively integrating (mostly) two-body terms[33,34] and whether they can resolve the structural degeneracy issues discussed in Ref. [31].

In this Letter, motivated by physical intuition, we derive a recursively embedded atom neural network (REANN) model that naturally integrates the message-passing concept into a well-defined local descriptor. Numerical results show that this REANN model easily addresses the distinguishability challenge proposed in Ref. [31] and incorporates some nonlocal effects. More importantly, we formally prove that the REANN model can formulate a complete representation of the local environment in a highly efficient way without explicitly including high-order correlations.

Let us start with the original embedded atom neural network (EANN) model which takes the atomistic representation of total energy and encodes the information of local environment by the invariant embedded density descriptor[23]. For simplicity, an embedded density invariant ( $\rho_i$ ) at the position of atom  $i$  is given by the square of the linear combination of atomic orbitals of its neighbors,

$$\rho_i = \sum_{l_x, l_y, l_z}^{l_x+l_y+l_z=L} \frac{L!}{l_x!l_y!l_z!} \left[ \sum_{j \neq i}^{N_c} c_j \varphi(\hat{\mathbf{r}}_{ij}) f_c(r_{ij}) \right]^2, \quad (1)$$

where  $\hat{\mathbf{r}}_{ij} = \hat{\mathbf{r}}_i - \hat{\mathbf{r}}_j$ , with  $\hat{\mathbf{r}}_i = (x_i, y_i, z_i)$  and  $\hat{\mathbf{r}}_j = (x_j, y_j, z_j)$  being the Cartesian coordinate vectors of the central atom  $i$  and a neighbor atom  $j$ ,  $r_{ij} = |\hat{\mathbf{r}}_{ij}|$  is the distance between them,  $\varphi(\hat{\mathbf{r}}_{ij})$  is the Gaussian-type orbital centered at atom  $j$  parameterized by its center ( $r_s$ ), width ( $\alpha$ ), and angular momenta ( $l_x, l_y, l_z$ , and  $L = l_x+l_y+l_z$ ),

$$\varphi(\hat{\mathbf{r}}_{ij}) = (x_i - x_j)^{l_x} (y_i - y_j)^{l_y} (z_i - z_j)^{l_z} \exp\left[-\alpha (r_{ij} - r_s)^2\right], \quad (2)$$

$f_c(r_{ij})$  is a cutoff function continuously damping the invariant to zero at the cutoff radius ( $r_c$ ), and  $N_c$  is the number of atoms within  $r_c$ . A set of  $\rho_i$  with different parameters are used as input of the atomic NNs and orbital coefficients ( $c_j$ ) are easily optimized along with the parameters of NNs.  $\rho_i$  has a clear physical meaning representing the density contribution from different type of atomic orbitals and expresses two- ( $L=0$ ) and three-body ( $L>0$ ) interactions in a uniform way. This can be seen by explicitly rewriting Eq. (1) in terms of interatomic distances and angles according to the multinomial theorem[23,35],

$$\rho_i = \sum_{j, k \neq i} c_j \exp\left[-\alpha (r_{ij} - r_s)^2\right] f_c(r_{ij}) c_k \exp\left[-\alpha (r_{ik} - r_s)^2\right] f_c(r_{ik}) r_{ij}^{L} r_{ik}^{-L} (\cos \theta_{ijk})^L. \quad (3)$$

Indeed, Eq. (1) allows the evaluation of three-body terms at a cost of two-body ones, resulting in a linear scaling with respect to  $N_c$ . As a result, this EANN model shows

better efficiency than many other descriptor-based MILPs[36] and good representability of energies[23] and tensorial properties[37,38].

We next take CH<sub>4</sub> as an illustrative example of local completeness. Like other incomplete descriptors, embedded density invariants and corresponding atomic energies of the C-center are identical, when two C-centered structures of CH<sub>4</sub> have the same list of distances and angles, as displayed in Fig. 1. This can be seen from Eq. (3) as orbital coefficients are fixed after training (like NNs' parameters) so that  $\rho_i$  are determined by these distances and angles only. However, considering the linear combination of atomic orbitals in Eq. (1) as an analog of a molecular orbital, it is a matter of fact in quantum chemistry that  $c_j$  should virtually vary with the molecular configuration. One simplest way to cast this physical concept into the descriptor is to make  $c_j$  itself a function of the  $j$ th atom's neighbor environment behaving like the atomic energy. In this scenario, orbital coefficients of the four H atoms in two CH<sub>4</sub> molecules can be different when their respective H-centered environments are different. This will give rise to nonequivalent C-centered embedded density invariants and atomic energies for the two local structures indistinguishable by three-body correlations, as clearly shown in Fig. 1. Importantly, atomic orbitals in the vicinity of atom  $j$  have been calculated for obtaining the atomic energy ( $E_j$ ), need not be recalculated in the evaluation of environment-dependent  $c_j$ .

Apparently, the orbital coefficient can be recursively embedded in this way whenever necessary and a generalized expression is,

$$c_j^t = g_j^{t-1} \left( \mathbf{p}_j^{t-1} \left( \mathbf{c}_j^{t-1}, \mathbf{r}_j^{t-1} \right) \right), \quad (4)$$

where  $\mathbf{c}_j^{t-1}$  and  $\mathbf{r}_j^{t-1}$  are the collections of orbital coefficients and atomic positions in the neighborhood of the central atom  $j$  in the  $(t-1)$ th iteration,  $\boldsymbol{\rho}_j^{t-1}$  is the corresponding embedded density feature vector,  $\mathbf{g}_j^{t-1}$  is an atomic NN mapping  $\boldsymbol{\rho}_j^{t-1}$  to  $c_j^t$ , namely the orbital coefficient of atom  $j$  as a neighbor of other atoms in the  $t$ th iteration. One may immediately realize that this is an effective message-passing formula[1], except that here the orbital coefficients, rather than the whole feature vector, iteratively pass the environmental information between an atom and its neighbors. This REANN model is schematically displayed in Fig. 2a. This is an intriguing result that makes a bridge, perhaps for the first time, between local many-body descriptors and the less physically intuitive message-passing features.

Next we turn to discuss how higher-order correlations are incorporated in this recursion, an issue rarely discussed in previous studies on MPNNs. Supposing that the iteration undergoes  $T$  times ( $T>0$ ), it is convenient to use a simplified version of Eq. (3),

$$\rho_i^T = \sum_{j,k} c_j^T c_k^T \mathcal{F}(r_{ij}, r_{ik}, r_{jk}), \quad (5)$$

where the orbital coefficients are now  $T$ -dependent ( $c_j^T$  and  $c_k^T$ ) and  $\mathcal{F}(r_{ij}, r_{ik}, r_{jk})$  represents a generalized three-body correlation term collecting these functions in Eq. (3). Substituting Eq. (4) into Eq. (5) and assuming no hidden layer in  $\mathbf{g}_j^{T-1}$  (*i.e.* a linear function), we have

$$\rho_i^T = \sum_{j,k} \mathcal{F}(r_{ij}, r_{ik}, r_{jk}) \sum_{n_1=1}^{N_\rho} w_{n_1} \rho_j^{T-1, n_1} \sum_{n_2=1}^{N_\rho} w_{n_2} \rho_k^{T-1, n_2}, \quad (6)$$

where  $w_{n_1}$  and  $w_{n_2}$  are linear weights of the corresponding features,  $N_\rho$  is the number of embedded density invariants. Note that using a nonlinear  $\mathbf{g}_j^{T-1}$  here would not alter our conclusion but will complicate this equation. We then substitute Eq. (5) in

the  $(T-1)$ th iteration back to Eq. (6) and reorder the summations,

$$\rho_i^T = \sum_{j,k} \sum_{n_1, n_2}^{N_p} w_{n_1} w_{n_2} \sum_{j_1, j_2} \sum_{k_1, k_2} c_{j_1}^{T-1, n_1} c_{j_2}^{T-1, n_1} c_{k_1}^{T-1, n_2} c_{k_2}^{T-1, n_2} \mathcal{F}(r_{ij}, r_{ik}, r_{jk}) \times \mathcal{F}(r_{jj_1}, r_{jj_2}, r_{j_1 j_2}) \mathcal{F}(r_{kk_1}, r_{kk_2}, r_{k_1 k_2}) \quad (7)$$

where  $j_1$  and  $j_2$ ,  $k_1$  and  $k_2$  are indexes of neighbor atoms of atom  $j$  and atom  $k$  respectively.

Summing up these atoms in Eq. (7) will cover atom  $i$  and its all neighbors. Consequently,

the product of the three  $\mathcal{F}$  functions will involve at most nine non-redundant

interatomic distances within the local environment of atom  $i$  given sufficient neighbors.

Eq. (7) effectively incorporates higher-order correlations than Eq. (5) in this way.

As the recursive update of orbital atoms till the last environment-independent ones,

the number of three-body functions doubles in each iteration, as illustrated in Fig. 2c.

This will make  $\rho_i^T$  eventually the sum of products of  $(2^{T+1}-1)$  three-body  $\mathcal{F}$

functions after  $T$  iterations, which can be generalized as,

$$\rho_i^T = \sum_m \eta_m \prod_{(i,j,k)}^{2^{T+1}-1} \mathcal{F}(r_{ij}, r_{ik}, r_{jk}), \quad (8)$$

where  $m$  collects all indexes of the summation,  $\eta_m$  is the collection of all weights and

orbital coefficients, and  $i, j, k$  span over all atomic indexes involved. According to

aforementioned discussion,  $\rho_i^T$  will contain at least one highest-order correlation term

with  $3(2^{T+1}-1)$  non-redundant interatomic distances in the neighborhood of atom  $i$  with

sufficient neighbors, along with some lower-order terms due to repeated interatomic

distances. Regarding atoms as nodes and interatomic distances as edges, the highest-

order correlation term can be viewed as an analog of the Eulerian path in graph theory

(a path in a finite graph passing every edge just once), except that in our case this path

can pass the same edge more than once. Fig. 2b illustrates such a path walking through



all edges in CH<sub>4</sub> after two iterations. More complex examples are given in the Supplementary Material (SM).

By definition, a complete many-body descriptor has to correlate all interatomic distances in the system[39]. This implies that  $\rho_i^T$  will involve a complete correlation of an atom-centered environment, if  $3(2^{T+1}-1) \geq N_c(N_c-1)/2$ . The minimum number of iterations to warrant this is thus given by  $T_{min} = \lceil \log_2 \{(N_c(N_c-1))/6+1\} \rceil$ , where  $\lceil \cdot \rceil$  rounds off the number to the nearest integer. Recall that the cost of each iteration scales linearly with  $N_c$  and atomic orbitals need be calculated only once. This is a striking finding that the local completeness in structural descriptors can be achieved with  $\sim O(\log_2 N_c)$  complexity, instead of the exponential scaling with the body-order when explicitly computing high-order correlations[32]. Our approach will be increasingly more favorable as  $N_c$  increases.

Similarly, this analysis can also estimate the required number of interaction blocks (or the time of message passed) in other MPNN representations, which was often empirically specified without a guidance. This number has to be greater than  $N_c(N_c-1)/2$ , theoretically, if only two-body features were recursively embedded (*e.g.* in SchNet[33]), because each iteration now introduces only one more interatomic distance towards the higher-body correlation. It is even worse is that using radial functions alone actually does not warrant the completeness, because atoms with distances greater than  $r_c$  cannot be correlated in any way and an example is given in the SM. It should be emphasized that while the above derivation is instructive, the practical implementation remains based on Eqs. (2) and (4) for numerical efficiency.

To validate our derivation numerically, we use the CH<sub>4</sub> dataset provided by Ceriotti and coworkers as a stringent test[31]. This dataset includes ~7.7 million configurations with randomly distributed atoms excluding structures with too close contacts. Due to the existence of near degenerate manifolds and many unphysical configurations with energies up to 70 eV, this dataset has been claimed to be the best touchstone of the representability and completeness of the descriptor. Since there are only five atoms in CH<sub>4</sub>, we estimate that many-body correlations become complete at  $T_{min} = 2$ . We have optimized  $r_s$ ,  $\alpha$ , and  $c_j$  together with all NN parameters, as readily implemented in PyTorch[40], yielding an end-to-end deep learning framework. To demonstrate the performance of the features themselves, we also train pure linear models by removing all hidden layers of NNs (both for orbital coefficients and energy prediction). Details of training are given in the SM.

Fig. 3a compare the test root-mean-square-errors (RMSEs) of various linear models as a function of the number of training configurations ( $n_{train}$ ). The learning curve of  $T=0$  (including three-body correlations only) exhibits a clear saturation with respect to  $n_{train}$ , which is fully consistent with the result of Ref. [31] using three-body power spectrum features. Recursively expanding orbital coefficients steepens the learning curve and reduces the error significantly. Even the result with only one iteration ( $T=1$ ) obviously outperforms that from Ref. [31] obtained with the mix of three- and four-body (3B+4B) correlations. With two iterations ( $T=2$ ), which are supposed to offer a complete correlation, we observe a saturated error of ~0.6 kcal/mol with  $10^6$  points. This result is in good agreement with that of Nigam *et al.*[32] who used an iterative

contraction algorithm to select up to five-body (5B) invariants (the highest-body correlation for CH<sub>4</sub>). These results clearly indicate the local completeness of our recursively embedded density descriptor.

Incorporating the nonlinearity by NNs substantially increases the flexibilities of all models. As shown in Fig 3b, 3B+4B correlations in Ref. [31] trained with 3 million points led to an RMSE of  $\sim 0.5$  kcal/mol. Impressively, our EANN model ( $T=0$ ) gives an even much lower learning curve, exhibiting its superior performance despite its three-body nature. The lower error may be due to the deeper NNs used in our EANN model, but one shall note that much fewer invariants are used as the input (45) here than that (2000) in Ref. [31]. As  $T$  increases, the test error further decreases, although the improvement from  $T=1$  to  $T=2$  is less significant than that from  $T=0$  to  $T=1$ . This is consistent with the fact that  $T=1$  already includes eight interatomic distances of CH<sub>4</sub> (see Fig. 2b) that are close to complete (10 distances in total). The test errors more or less converge at  $T=2$ , which are over one order of magnitude smaller than those with 3B+4B features[31], and those with the iteratively contracted features up to 5B[32].

An additional advantageous feature of the REANN model is its efficient description of some nonlocal effects, which allows using a smaller cutoff radius without loss of accuracy. This is because the correlations between atoms inside and outside the cutoff sphere have been implicitly encoded when iteratively updating orbital coefficients, as illustrated in Fig. 2a. We demonstrate this in bulk water, an important benchmark to demonstrate the power of MLIPs. We first use a dataset with 1593 structures of 64 water molecules computed by Cheng *et al.* [41] for developing a BPNN

potential[15]. The cutoff radius of BPNN potential was set long enough ( $r_c=6.2$  Å) to describe the strong hydrogen bond interactions. With a careful selection of symmetry functions, the reported RMSEs of the BPNN potential are comparable to those of the EANN model[36] with the same  $r_c$ , as listed in Table 1. Impressively, our REANN model ( $T=3$ ) greatly outperforms these two purely local descriptor-based counterparts, leading to an even slightly smaller RMSE for force with only about half of the cutoff radius ( $r_c=3$  Å). Apparently, this cutoff only incorporates the interactions between a water molecule and some nearest neighbors, while the correlations with the second neighboring shell are implicitly included by the message-passing way of updating orbital coefficients. The performance of the REANN model further improves with the increasing  $r_c$  and saturates at  $r_c\approx 5.5$  Å, yielding RMSEs (0.9 meV/atom for energies and 51.8 meV for forces) less than half of those of the BPNN potential. To avoid any data biases, we also test another dataset of water trained by Zhang *et al.* using the deep potential molecular dynamics (DPMD) method[18] with  $r_c=6.0$  Å. Our REANN model ( $T=2$ ) with  $r_c=4.5$  Å gives RMSEs of 0.2 meV/atom (energies) and 15.9 meV/Å (forces), again less than half of the reported values in Ref. [18]. These results suggest that some long-range interactions that are absent in those local descriptors due to the limited cutoff can increase the reliability of the model.

Summarizing, we propose a physically-motivated adaption of the local descriptor-based EANN model to generate the REANN model and reveal its connection with other MPNNs often inspired from graph neural network. We formally derive that how many-body correlations are introduced by iteratively passing messages (updating orbital

coefficients here) and prove that this is a highly-efficient way to achieve a complete description of the local environment, without explicitly computing high-order features. Numerical tests demonstrate the local completeness and nonlocality of the REANN model, warranting its high accuracy among existing ML models. Our strategy can be easily adapted to improve other sophisticated local descriptor-based MLIP models, for example, by making atomic weights of the weighted atom-centered symmetry functions variable with its local environment[26] or adding such learnable coefficients to the DPMD descriptors[18]. We believe this will open a new window for developing more accurate and efficient MLIPs for atomistic simulations of more complicated systems.

**Data Availability:** All training data can be found in the original publications. Our Pytorch-based NN potentials for tests will be made public after the manuscript is accepted.

**Acknowledgement:** This work is supported by National Key R&D Program of China (2017YFA0303500), National Natural Science Foundation of China (22073089 and 22033007), Anhui Initiative in Quantum Information Technologies (AHY090200), and The Fundamental Research Funds for the Central Universities (WK2060000017). Calculations have been done on the Supercomputing Center of USTC.

## References:

- [1] O. T. Unke, S. Chmiela, H. E. Saucedo, M. Gastegger, I. Poltavsky, K. T. Schütt, A. Tkatchenko, and K.-R. Müller, *Chem. Rev.* (2021).
- [2] K. Shao, J. Chen, Z. Zhao, and D. H. Zhang, *J. Chem. Phys.* **145**, 071101 (2016).
- [3] B. Jiang, J. Li, and H. Guo, *Int. Rev. Phys. Chem.* **35**, 479 (2016).
- [4] S. Manzhos, R. Dawes, and T. Carrington Jr., *Int. J. Quant. Chem.* **115**, 1012 (2015).
- [5] S. Chmiela, A. Tkatchenko, H. E. Saucedo, I. Poltavsky, K. T. Schütt, and K. R. Müller, *Sci. Adv.* **3**, e1603015 (2017).
- [6] K. T. Schütt, F. Arbabzadah, S. Chmiela, K. R. Müller, and A. Tkatchenko, *Nat. Comm.* **8**, 13890 (2017).
- [7] J. S. Smith, O. Isayev, and A. E. Roitberg, *Chem. Sci.* **8**, 3192 (2017).
- [8] C. Qu, Q. Yu, and J. M. Bowman, *Annu. Rev. Phys. Chem.* **69**, 151 (2018).
- [9] S. Manzhos and T. Carrington, *Chem. Rev.* (2020).
- [10] B. Jiang, J. Li, and H. Guo, *J. Phys. Chem. Lett.* **11**, 5120 (2020).
- [11] W.-K. Chen, X.-Y. Liu, W.-H. Fang, P. O. Dral, and G. Cui, *J. Phys. Chem. Lett.* **9**, 6702 (2018).
- [12] J. Westermayr, M. Gastegger, M. Menger, S. Mai, L. Gonzalez, and P. Marquetand, *Chem. Sci.* **10**, 8100 (2019).
- [13] Y. Guan, D. H. Zhang, H. Guo, and D. R. Yarkony, *Phys. Chem. Chem. Phys.* **21**, 14205 (2019).
- [14] J. Westermayr and P. Marquetand, *Chem. Rev.* (2020).
- [15] J. Behler and M. Parrinello, *Phys. Rev. Lett.* **98**, 146401 (2007).
- [16] A. P. Bartók, M. C. Payne, R. Kondor, and G. Csányi, *Phys. Rev. Lett.* **104**, 136403 (2010).
- [17] A. P. Bartók, S. De, C. Poelking, N. Bernstein, J. R. Kermode, G. Csányi, and M. Ceriotti, *Sci. Adv.* **3**, e1701816 (2017).
- [18] L. Zhang, J. Han, H. Wang, R. Car, and W. E, *Phys. Rev. Lett.* **120**, 143001 (2018).
- [19] S. D. Huang, C. Shang, X. J. Zhang, and Z. P. Liu, *Chem. Sci.* **8**, 6327 (2017).
- [20] B. Jiang and H. Guo, *J. Chem. Phys.* **141**, 034109 (2014).
- [21] J. Behler, *J. Chem. Phys.* **134**, 074106 (2011).
- [22] A. P. Bartók, R. Kondor, and G. Csányi, *Phys. Rev. B* **87**, 184115 (2013).
- [23] Y. Zhang, C. Hu, and B. Jiang, *J. Phys. Chem. Lett.* **10**, 4962 (2019).
- [24] M. J. Willatt, F. Musil, and M. Ceriotti, *J. Chem. Phys.* **150**, 154110 (2019).
- [25] F. A. Faber, A. S. Christensen, B. Huang, and O. A. von Lilienfeld, *J. Chem. Phys.* **148**, 241717 (2018).
- [26] M. Gastegger, L. Schwiedrzik, M. Bittermann, F. Berzsényi, and P. Marquetand, *J. Chem. Phys.* **148**, 241709 (2018).
- [27] A. V. Shapeev, *Multiscale Model. Simul.* **14**, 1153 (2016).
- [28] R. Drautz, *Phys. Rev. B* **99**, 014104 (2019).
- [29] A. E. A. Allen, G. Dusson, C. Ortner, and G. Csányi, *Mach. Learn.: Sci. Technol.* **2**, 025017 (2021).
- [30] S. D. Huang, C. Shang, P. L. Kang, and Z. P. Liu, *Chem. Sci.* **9**, 8644 (2018).
- [31] S. N. Pozdnyakov, M. J. Willatt, A. P. Bartók, C. Ortner, G. Csányi, and M. Ceriotti, *Phys. Rev. Lett.* **125**, 166001 (2020).
- [32] J. Nigam, S. Pozdnyakov, and M. Ceriotti, *J. Chem. Phys.* **153**, 121101 (2020).
- [33] K. T. Schütt, H. E. Saucedo, P.-J. Kindermans, A. Tkatchenko, and K.-R. Müller, *J. Chem. Phys.* **148**, 241722 (2018).

- [34] O. T. Unke and M. Meuwly, *J. Chem. Theory Comput.* **15**, 3678 (2019).
- [35] A. Takahashi, A. Seko, and I. Tanaka, *Phys. Rev. Mater.* **1**, 063801 (2017).
- [36] Y. Zhang, C. Hu, and B. Jiang, *Phys. Chem. Chem. Phys.* **23**, 1815 (2021).
- [37] Y. Zhang, R. J. Maurer, and B. Jiang, *J. Phys. Chem. C* **124**, 186 (2020).
- [38] Y. Zhang, S. Ye, J. Zhang, C. Hu, J. Jiang, and B. Jiang, *J. Phys. Chem. B* **124**, 7284 (2020).
- [39] E. Josué Landinez Borda and A. Samanta, arXiv:2004.14442 (2020).
- [40] A. Paszke *et al.*, in *Advances in Neural Information Processing Systems 32 (NeurIPS 2019)*, edited by H. Wallach *et al.* (Curran Associates Inc., Vancouver, Canada, 2019).
- [41] B. Cheng, E. A. Engel, J. Behler, C. Dellago, and M. Ceriotti, *Proc. Natl. Acad. Sci. U.S.A.* **116**, 1110 (2019).

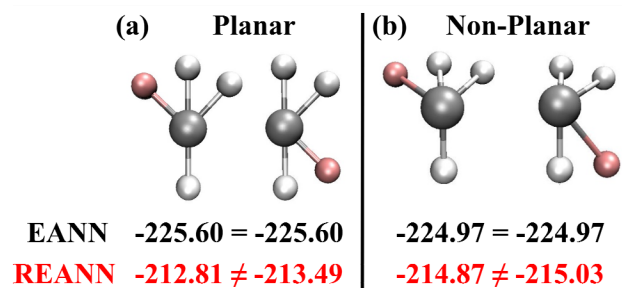


Fig.1 Two representative pairs of CH<sub>4</sub> molecules that have the same set of distances and angles between central C atom (silver) and neighboring H atoms (white for identical ones and light red for the different one), for which the EANN (REANN) atomic energies for C are identical (distinct).



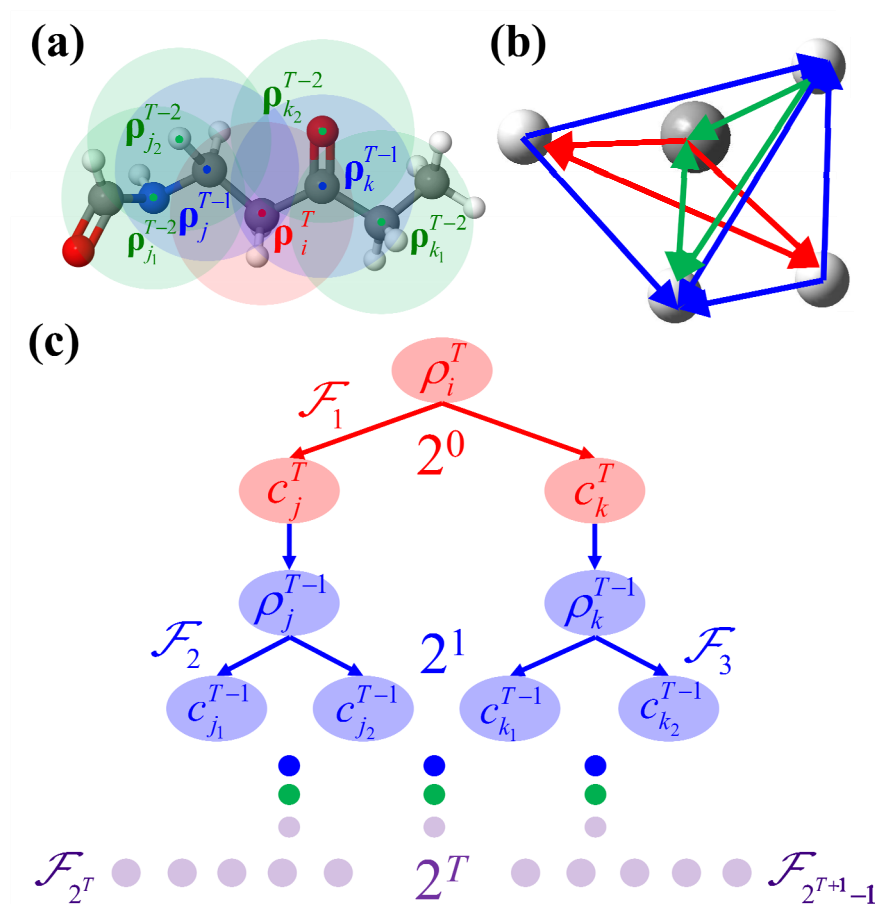


Fig. 2 (1) Schematic diagram of the REANN model showing how the density descriptor is recursively embedded. (b) An example in  $\text{CH}_4$  showing how the body-order of correlations (the number of interatomic distances) is increased along with recursion. (c) An illustration that how the number of three-body interaction terms increases in each iteration ( $2^T$ ). Different colors correspond to different iteration times, namely  $T=0$  (red),  $T=1$  (blue),  $T=2$  (green).

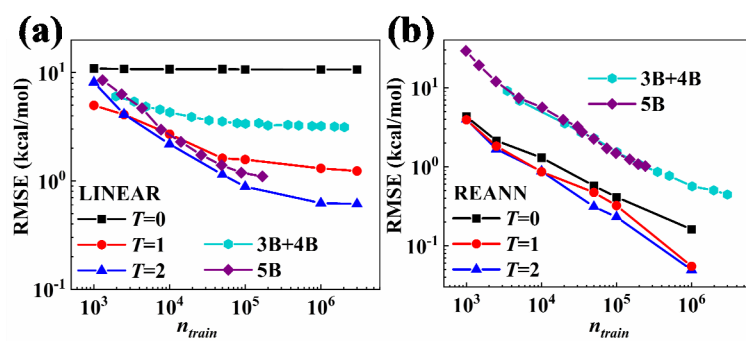


Fig. 3 (a) Comparison of the RMSEs for energies of random CH<sub>4</sub> configurations of linear fits in Refs. [31] (with 3B+4B correlations) and [32] (with 5B correlation), and that with the recursively embedded density descriptor ( $T=0, 1, 2$ ) (b) Similar to (a) but all results are now based on nonlinear NN fits.

Table 1: Test RMSEs of energies and forces for bulk water using the dataset in Ref [41].

$r_c$ (Å)	REANN					EANN*	BPNN
	3.0	3.5	4.5	5.5	6.2	6.2	6.2
Energy (meV/atom)	2.8	1.5	1.1	0.9	0.8	2.1	2.3
Force (meV/ Å)	104.4	73.1	58.0	51.1	53.2	129.0	120

\*Taken from Ref. [36]